

Mechanism of selective benzene hydroxylation catalyzed by iron-containing zeolites

Benjamin E. R. Snyder^{a,1}, Max L. Bols^b, Hannah M. Rhoda^a, Pieter Vanelderen^{a,b}, Lars H. Böttger^a, Augustin Braun^a, James J. Yan^a, Ryan G. Hadt^{a,2}, Jeffrey T. Babicz Jr.^a, Michael Y. Hu^c, Jiyong Zhao^c, E. Ercan Alp^c, Britt Hedman^d, Keith O. Hodgson^{a,d}, Robert A. Schoonheydt^{b,3}, Bert F. Sels^{b,3}, and Edward I. Solomon^{a,d,3}

^aDepartment of Chemistry, Stanford University, Stanford, CA 94305; ^bDepartment of Microbial and Molecular Systems, Centre for Surface Chemistry and Catalysis, Katholieke Universiteit Leuven, B-3001 Leuven, Belgium; ^cAdvanced Photon Source, Argonne National Laboratory, Argonne, IL 60439; and ^dStanford Synchrotron Radiation Lightsource, SLAC National Accelerator Laboratory, Stanford University, Menlo Park, CA 94025

Edited by Alexis T. Bell, University of California, Berkeley, CA, and approved October 18, 2018 (received for review August 22, 2018)

A direct, catalytic conversion of benzene to phenol would have wide-reaching economic impacts. Fe zeolites exhibit a remarkable combination of high activity and selectivity in this conversion, leading to their past implementation at the pilot plant level. There were, however, issues related to catalyst deactivation for this process. Mechanistic insight could resolve these issues, and also provide a blueprint for achieving high performance in selective oxidation catalysis. Recently, we demonstrated that the active site of selective hydrocarbon oxidation in Fe zeolites, named α -O, is an unusually reactive Fe(IV)=O species. Here, we apply advanced spectroscopic techniques to determine that the reaction of this Fe(IV)=O intermediate with benzene in fact regenerates the reduced Fe(II) active site, enabling catalytic turnover. At the same time, a small fraction of Fe(III)-phenolate poisoned active sites form, defining a mechanism for catalyst deactivation. Density-functional theory calculations provide further insight into the experimentally defined mechanism. The extreme reactivity of α -O significantly tunes down (eliminates) the rate-limiting barrier for aromatic hydroxylation, leading to a diffusion-limited reaction coordinate. This favors hydroxylation of the rapidly diffusing benzene substrate over the slowly diffusing (but more reactive) oxygenated product, thereby enhancing selectivity. This defines a mechanism to simultaneously attain high activity (conversion) and selectivity, enabling the efficient oxidative upgrading of inert hydrocarbon substrates.

zeolites | spectroscopy | catalysis

The direct conversion of benzene to phenol remains an outstanding challenge in modern chemistry (1). Fe zeolites exhibit remarkable performance in this application, hydroxylating benzene catalytically with 95+% selectivity for phenol—even at high levels of conversion (30–45%) (2–6). This is the critical step in the AlphOx process of Panov, implemented in a Solutia pilot plant (2–5). Catalyst deactivation at elevated temperature remains a crucial problem (4, 7, 8). Mechanistic insight could resolve this issue, and provide a blueprint for developing selective oxidation catalysts with high reactivity and selectivity. However, despite three decades of effort, direct experimental data clarifying the catalytic mechanism are limited (9). We recently showed the active site of selective hydrocarbon hydroxylation, called α -Fe(II) (2), is a mononuclear $S = 2$ square planar Fe(II) center (10, 11). α -Fe(II) is activated by nitrous oxide to form α -O (2), a mononuclear square pyramidal $S = 2$ Fe(IV)=O intermediate with a constrained coordination geometry that imparts exceptional reactivity, enabling H-atom abstraction from CH_4 at room temperature (10, 11). In this study, we investigate the single-turnover reactivity of α -O with C_6H_6 using advanced spectroscopic techniques from bioinorganic chemistry. Spectroscopic data show the reduced α -Fe(II) active site is regenerated following single turnover. The phenol product is thus released from the active site quantitatively at room temperature, but not overoxidized. At the same time, we find a small fraction of

partially oxidized, deactivated Fe(III)-phenolate sites are generated. These data, coupled to density-functional theory (DFT) calculations, define a catalytic mechanism leading to high activity (conversion) and selectivity, along with a competing mechanism leading to catalyst deactivation.

Results and Discussion

Defining the Product of Single Turnover. Direct experimental data tracking the state of the α -O active site in its reaction with benzene are lacking. We therefore used Mössbauer spectroscopy as a quantitative probe of iron speciation in iron-exchanged zeolite beta (Fe-BEA) under single-turnover conditions. As shown in Fig. 1A, reacting α -O in Fe-BEA (gray trace) with C_6H_6 vapor at room temperature results in the quantitative formation of a C_6H_6 species labeled α - C_6H_6 (red trace) with 6K Mössbauer parameters characteristic of high spin ($S = 2$) Fe(II) (isomer shift, IS; quadrupole splitting, QS; IS = 1.30, QS = 3.90), but distinct from those previously defined for α -Fe(II) (precursor to α -O; blue trace) (10, 11). The larger quadrupole splitting of α - C_6H_6 indicates this site no longer has the square planar geometry of α -Fe(II), suggesting an axial ligand is now present.

Significance

Fe zeolites are heterogeneous catalysts that show potential in a number of important industrial applications, including the selective partial oxidation of methane to methanol at room temperature, and the selective conversion of benzene to phenol. There are practical limitations associated with Fe-zeolite catalysts that may be resolved with mechanistic insight; however, reliable experimental data on Fe zeolites are limited. This study defines the mechanism of selective benzene hydroxylation catalyzed by Fe zeolites, clarifying the relationship between active site structure and catalytic performance (activity, selectivity). Mechanistic insight from this study represents an important step toward synthetic control over function in selective hydrocarbon oxidation catalysis.

Author contributions: B.E.R.S., R.A.S., B.F.S., and E.I.S. designed research; B.E.R.S., M.L.B., H.M.R., P.V., L.H.B., A.B., J.J.Y., R.G.H., J.T.B., M.Y.H., J.Z., and E.E.A. performed research; B.E.R.S., B.H., K.O.H., R.A.S., B.F.S., and E.I.S. analyzed data; and B.E.R.S., R.A.S., B.F.S., and E.I.S. wrote the paper.

The authors declare no conflict of interest.

This article is a PNAS Direct Submission.

Published under the PNAS license.

¹Present address: Department of Chemistry, University of California, Berkeley, CA 94720.

²Present address: Division of Chemistry and Chemical Engineering, California Institute of Technology, Pasadena, CA 91125.

³To whom correspondence may be addressed. Email: robert.schoonheydt@biw.kuleuven.be, bert.sels@biw.kuleuven.be, or edward.solomon@stanford.edu.

This article contains supporting information online at www.pnas.org/lookup/suppl/doi:10.1073/pnas.1813849115/-DCSupplemental.

125
126
127
128
129
130
131
132
133
134
135
136
137
138
139
140
141
142
143
144
145
146
147
148
149
150
151
152
153
154
155
156
157
158
159
160
161
162
163
164
165
166
167
168
169
170
171
172
173
174
175
176
177
178
179
180
181
182
183
184
185
186
Q:27
Q:11

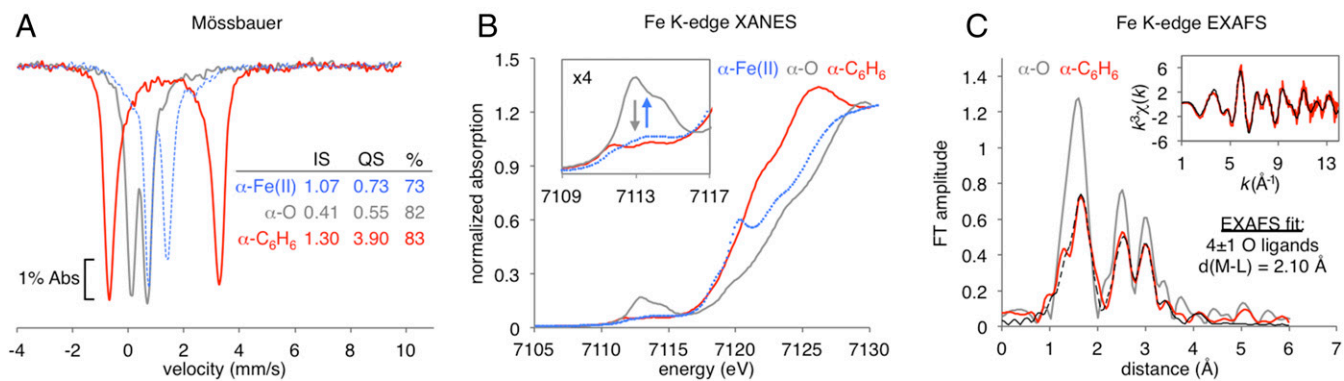


Fig. 1. (A) ^{57}Fe Mössbauer spectrum of α -O in Fe-BEA (82%, gray trace) collected at 6K, compared with data collected after its reaction with C_6H_6 , forming α -C₆H₆ (83% red trace). Past data (11) from the reduced α -Fe(II) active site are included for reference (73%, blue trace). (B) Fe K-edge X-ray absorption near-edge spectra of α -O (gray trace) and α -C₆H₆ (red trace), showing an ~ 3 -eV downshift in the rising edge coupled to loss of the intense pre-edge features of α -O (Inset). Past data (11) from α -Fe(II) are included for reference (blue trace). (C) Comparison of FT EXAFS spectra of α -O (gray trace) and α -C₆H₆ (red trace, with fit in dashed black). (Inset) The EXAFS spectrum of α -C₆H₆ (experimental data: red; fit: dashed black), with the first shell fit summarized below. The full EXAFS fit is presented in *SI Appendix*, Fig. S2.

To define the ligation of α -C₆H₆, we employed a combination of Fe K-edge X-ray absorption spectroscopy (XAS) coupled to ^{57}Fe Fe nuclear resonance vibrational spectroscopy (NRVS). NRVS is a synchrotron-based technique that selectively probes vibrations of Fe sites in metalloenzymes and zeolites (11, 12). Importantly, NRVS and XAS are sensitive to $S = 2$ Fe(II) centers, which can be difficult (or impossible) to resolve in optical absorption, resonance Raman, and electron paramagnetic resonance spectroscopy. As shown in the X-ray absorption near-edge region in Fig. 1B, the reaction of α -O (gray trace) with C_6H_6 (red trace) results in loss of the intense α -O pre-edge features at 7,110–7,115 eV (Inset), as well as a downshift in the rising edge energy by ~ 3 eV. These changes are consistent with reduction of α -O to an Fe(II) species distinct from α -Fe(II) (blue trace, with a low-energy 1s–4p transition at 7,120 eV that is characteristic of square planar geometry) (11). In the extended X-ray absorption fine structure (EXAFS) region in Fig. 1C, the Fourier transform (FT) shows a loss of first-shell intensity moving from α -O (gray) to α -C₆H₆ (red). Comparing the first-shell EXAFS fits of α -C₆H₆ in Fig. 1C and of α -O from Snyder et al. (11) shows this is due to loss of the short 1.63-Å scattering path from the reactive terminal oxo ligand (see *SI Appendix*, Fig. S2 for full EXAFS fits). The first coordination sphere of α -C₆H₆ was fit with 4 ± 1 oxygen ligands at 2.10 Å. However, the EXAFS fit does not clarify the nature of the axial ligand. (See *SI Appendix*, Fig. S2; this ligand could contribute to the 2.10-Å shell or, alternatively, be weakly bound and not significantly contribute to the experimental data.)

To resolve this ambiguity, we directly synthesized candidates for α -C₆H₆ by binding either phenol (product) or C_6H_6 (substrate, present in excess under reaction conditions) to α -Fe(II). As shown in *SI Appendix*, Fig. S1, in each case this leads to quantitative conversion of α -Fe(II) to a new $S = 2$ Fe(II) species with Mössbauer parameters that are highly similar to α -C₆H₆. However, XAS and NRVS data presented in Fig. 2 show significant differences for benzene- and phenol-ligated α -Fe(II). FT EXAFS data in Fig. 2A show excess first-shell intensity for the phenol-bound site (black trace; see 1–2-Å region) relative to α -C₆H₆ (red trace). The EXAFS fit given in the inset indicates this is due to the presence of a fifth oxygen ligand at 2.09 Å. The XANES region presented in *SI Appendix*, Fig. S2 shows the phenol-bound site also does not reproduce the α -C₆H₆ pre-edge or rising edge. Finally, as shown in Fig. 2B, the phenol-bound site (black trace) does not reproduce the distribution of NRVS intensity for α -C₆H₆ (red trace) in the 0–250-cm⁻¹ region, which contains FeL₅ core modes that are highly sensitive to

coordination geometry (11). In this region, α -C₆H₆ shows a distinct peak at 165 cm⁻¹, while the phenol-bound site has a plateau from 165 to 210 cm⁻¹. The experimental Mössbauer, EXAFS, and NRVS data of the phenol-bound site are reproduced by the $S = 2$ Fe(II) DFT model presented in *SI Appendix*, Fig. S3. Alternatively, EXAFS data in Fig. 2C, NRVS data in Fig. 2D, and XANES data in *SI Appendix*, Fig. S2 demonstrate the spectroscopic features of C_6H_6 -ligated α -Fe(II) (blue traces) overlay with the features of α -C₆H₆ (red traces). The experimental

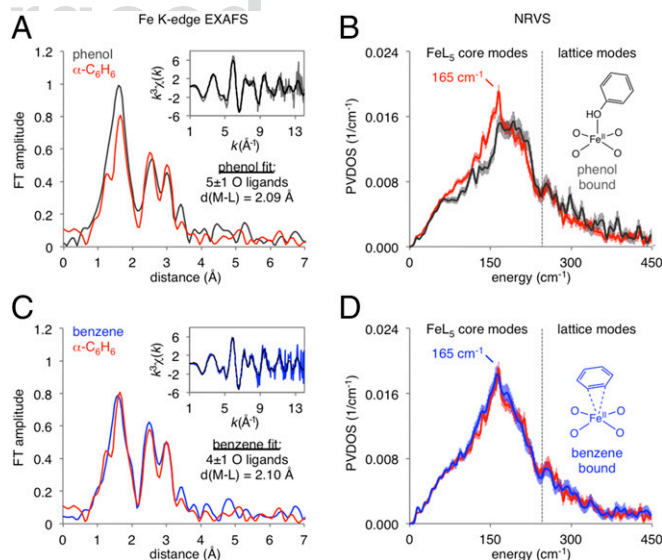


Fig. 2. (A) Comparison of FT EXAFS of α -C₆H₆ (red trace) and phenol-bound α -Fe(II) (dark-gray trace). (Inset) The phenol-bound k^3 -weighted EXAFS is shown (solid gray, fit in dashed black), with the first shell fit parameters given below. (B) Comparison of NRVS spectra of α -C₆H₆ (red trace) and phenol-bound α -Fe(II) (dark-gray trace). A structural model of the phenol-bound site is illustrated at the right of the figure, based on correlation of spectroscopy to DFT (*SI Appendix*, *SI Methods*). (C) Comparison of FT EXAFS of α -C₆H₆ (red trace) and benzene-bound α -Fe(II) (blue trace). (Inset) The benzene-bound k^3 -weighted EXAFS is shown (solid red, fit in dashed black), with the first shell fit parameters given below. (D) Comparison of NRVS spectra of α -C₆H₆ (red trace) and benzene-bound α -Fe(II) (blue trace). A structural model of the benzene-bound site, based on correlation of spectroscopy to DFT (*SI Appendix*, *SI Methods*), is illustrated at the right of the figure.

187
188
189
190
191
192
193
194
195
196
197
198
199
200
201
202
203
204
205
206
207
208
209
210
211
212
213
214
215
216
217
218
219
220
221
222
223
224
225
226
227
228
229
230
231
232
233
234
235
236
237
238
239
240
241
242
243
244
245
246
247
248

249
250
251
252
253
254
255
256
257
258
259
260
261
262
263
264
265
266
267
268
269
270
271
272
273
274
275
276
277
278
279
280
281
282
283
284
285
286
287
288
289
290
291
292
293
294
295
296
297
298
299
300
301
302
303
304
305
306
307
308
309
310
311
312
313
314
315
316
317
318
319
320
321
322
323
324
325
326
327
328
329
330
331
332
333
334
335
336
337
338
339
340
341
342
343
344
345
346
347
348
349
350
351
352
353
354
355
356
357
358
359
360
361
362
363
364
365
366
367
368
369
370
371
372

Mössbauer, EXAFS, and NRVS spectroscopy of α -C₆H₆ are reproduced by an $S = 2$ DFT model of α -Fe(II) with a weakly bound π - η^2 -C₆H₆ ligand (see *SI Appendix*, Fig. S3 for detail). As shown in *SI Appendix*, Fig. S4, the C₆H₆ ligand desorbs from α -C₆H₆ at room temperature, consistent with a weak bonding interaction.

The quantitative conversion of α -O to the substrate-bound reduced active site at room temperature has significant mechanistic implications. α -C₆H₆ is not a reaction intermediate, and its formation requires α -Fe(II) to release the phenol product before binding the excess C₆H₆ in the reactant stream. These results contradict earlier studies suggesting product desorption from the active site is rate limiting (13, 14), and/or driven by subsequent activation of N₂O (2, 14). High temperatures are therefore not required to regenerate the active site, but do assist in the subsequent desorption of phenol from the zeolite lattice [see temperature-programmed desorption (TPD) data in *SI Appendix*, Fig. S5]. The absence of overoxidized products (2, 3) indicates the released phenol does not go on to react with α -O. Interestingly, α -O does react directly with phenol vapor at room temperature to form diphenols—see *SI Appendix*, Fig. S6 and ref. 15. This suggests the benzene substrate is able to outcompete the phenol product, despite its lower activation toward electrophilic aromatic substitution reactions. The reactivity of α -O is therefore different from other mononuclear Fe(IV)=O intermediates: α -O achieves high levels of selectivity (95+%) at high levels of conversion (40+%) (6), while other Fe(IV)=O intermediates attain lower levels of selectivity (0–70%) at lower levels of conversion (<10%) (16–18). The clean regeneration of the α -Fe(II) active site following aromatic hydroxylation also raises an important contrast to methane hydroxylation in Fe zeolites, which is not catalytic (9), and where past Mössbauer studies show single-turnover results in a heterogeneous distribution of Fe species (*SI Appendix*, Fig. S7) (10). DFT studies presented below clarify the unique features of α -O leading to its unusually high reactivity and selectivity in aromatic hydroxylation.

A Mechanism Leading to Catalyst Deactivation. The regeneration of α -Fe(II) following aromatic hydroxylation in Fe-BEA contrasts with studies of Fe-ZSM-5, where phenolate-ligated products are proposed (19–22). A C₆H₆/ α -O formed spectroscopic product with a broad absorption band at 13,900 cm⁻¹ has been identified in Fe-ZSM-5, assigned as a binuclear Fe(III)-phenolate species based on rR data (20). This is proposed to be either a catalytic intermediate, a poisoned state of the active site, and/or precursor to coke formation (19–23). We used a range of spectroscopies to clarify the nature of this putative Fe(III) phenolate and its relation to the α -O active site. Mössbauer spectra in *SI Appendix*, Fig. S8 show the reaction of C₆H₆ with Fe-ZSM-5 parallels the Fe-BEA reaction, resulting in near-quantitative formation of a single Fe(II) product, with <5% Fe(III) present. However, as shown in Fig. 3, this also results in the 13,900-cm⁻¹ Abs band assigned to an Fe(III)₂ phenolate by Xia et al. (20) (Fig. 3A).

Tuning a laser into the 13,900-cm⁻¹ absorption feature enhances a number of Raman vibrations shown in Fig. 3B, with frequencies and intensities consistent with those in ref. 20. Reacting ¹⁸O-labeled α -O (see ref. 24 and *Materials and Methods*) with C₆H₆ results in the rR isotope shifts given in parentheses in Fig. 3B, which are diagnostic of a bound phenolate ligand. (An analogous 15,200-cm⁻¹ Abs feature forms in Fe-BEA—see *SI Appendix*, Fig. S8. Issues with fluorescence precluded rR studies of this system.) ¹⁸O label incorporation indicates the phenolate ligand is correlated with the active site (i.e., unrelated to spectator sites).

We used variable-temperature variable-field magnetic circular dichroism (VTVH-MCD) (9, 25) to define the electronic structure of this phenolate-bound species. As shown in Fig. 3C, the 13,900-cm⁻¹ Room-temperature (RT) Abs band resolves into

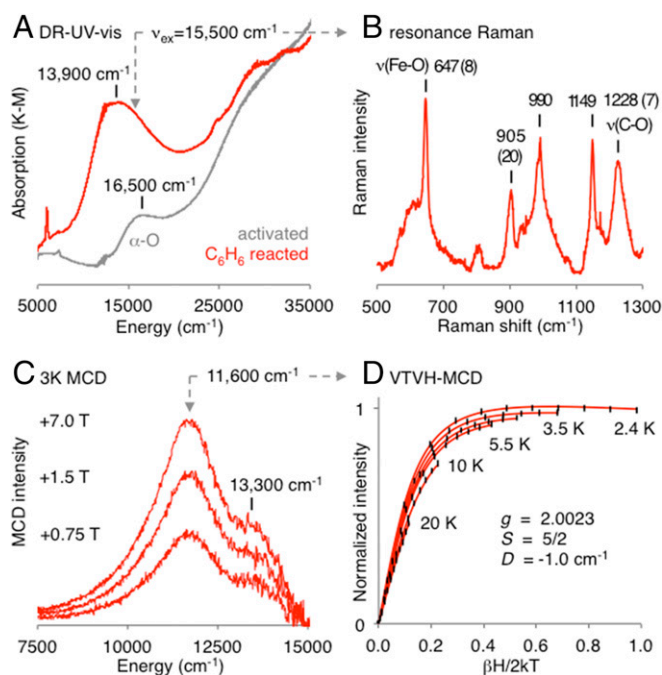


Fig. 3. (A) DR-UV-vis spectra of α -O in Fe-ZSM-5 (gray) and α -C₆H₆ (red), showing the appearance of an intense 13,900-cm⁻¹ band. (B) rR data from laser excitation into the high-energy shoulder of the 13,900-cm⁻¹ band, showing vibrations with frequencies and corresponding ¹⁸O isotope shifts (given in parentheses) characteristic of a phenolate ligand. The Fe-O and C-O stretching modes are indicated. (C) 3K variable-field MCD spectra of C₆H₆-reacted Fe-ZSM-5. (D) VTVH-MCD isotherms from the 11,600-cm⁻¹ MCD band (± 1 - σ error bars in black; spin Hamiltonian fit in red), and associated spin Hamiltonian parameters.

two components at 11,600 cm⁻¹ and 13,300 cm⁻¹ in 3K MCD spectroscopy. VTVH-MCD isotherms collected from these bands overlay within error, suggesting they derive from the same species. The 11,600-cm⁻¹ VTVH-MCD isotherms in Fig. 3D require a spin-Hamiltonian fit with an $S = 5/2$ ground state, consistent with a high-spin mononuclear Fe(III) phenolate [but not an oxo- or hydroxo-bridged 2Fe(III) site, which would have an integer-spin, likely singlet ground state (26)]. Compared with other mononuclear $S = 5/2$ Fe(III) phenolates, the 647-cm⁻¹ Fe-O-C₆H₅ stretching frequency from rR is high [typically 570–620 cm⁻¹ for $S = 5/2$ Fe(III) phenolates] (27, 28), indicating a strong binding interaction. Finally, the reaction of α -O with phenol results in >95% regeneration of Fe(II) (*SI Appendix*, Fig. S6), and the formation of diphenols (15). The small amount of Fe(III) phenolate that forms during the benzene reaction is therefore unrelated to small contributions from overoxidation. Site-selective spectroscopy therefore characterizes the geometric and electronic structure of this $S = 5/2$ Fe(III) phenolate, and shows this is a poisoned state of the α -Fe(II) active site generated during productive turnover. The absence of an Fe(III) signal in Mössbauer indicates <5% of sites are poisoned following single turnover, while analysis of DR-UV-vis band intensities indicates >0.2% poisoning (see *Materials and Methods* for detail). This would lead to 20–100% deactivation after 100 turnovers. DFT calculations presented below suggest phenolate poisoning occurs via H-atom loss from a bound catalytic intermediate.

A Mechanism Enabling High Reactivity and Selectivity. To define features of α -O contributing to its high reactivity and selectivity in aromatic hydroxylation, we constructed a DFT reaction coordinate that cleanly regenerates the reduced α -Fe(II) active

CHEMISTRY

- 621 27. Pyrz JW, Roe AL, Stern LJ, Que L, Jr (1985) Model studies of iron-tyrosinate proteins. *J Am Chem Soc* 107:614–620.
- 622
- 623 28. Carrano CJ, Carrano MW, Sharma K, Backes G, Sanders-Loehr J (1990) Resonance
- 624 Raman spectra of high- and low-spin ferric phenolates. Models for dioxygenases and
- 625 nitrile hydratase. *Inorg Chem* 29:1865–1870.
- 626 29. Fitzpatrick PF (2003) Mechanism of aromatic amino acid hydroxylation. *Biochemistry*
- 627 42:14083–14091.
- 628 30. Neidig ML, et al. (2006) Spectroscopic and electronic structure studies of aromatic
- 629 electrophilic attack and hydrogen-atom abstraction by non-heme iron enzymes. *Proc*
- 630 *Natl Acad Sci USA* 103:12966–12973.
- 631 31. Bassan A, Blomberg MR, Siegbahn PE (2003) Mechanism of aromatic hydroxylation by
- 632 an activated FeIV=O core in tetrahydrobiopterin-dependent hydroxylases. *Chemistry*
- 633 9:4055–4067.
- 634
- 635 32. Nam W (2007) High-valent iron(IV)-oxo complexes of heme and non-heme ligands in
- 636 oxygenation reactions. *Acc Chem Res* 40:522–531.
- 637 33. Vallee BL, Williams RJ (1968) Metalloenzymes: The entatic nature of their active sites.
- 638 *Proc Natl Acad Sci USA* 59:498–505.
- 639 34. Guroff G, et al. (1967) Hydroxylation-induced migration: The NIH shift. Recent ex-
- 640 periments reveal an unexpected and general result of enzymatic hydroxylation of
- 641 aromatic compounds. *Science* 157:1524–1530.
- 642 35. Dubkov KA, et al. (1997) Kinetic isotope effects and mechanism of biomimetic ox-
- 643 idation of methane and benzene on FeZSM-5 zeolite. *J Mol Catal Chem* 123:
- 644 155–161.
- 645 36. Moore RM, Katzer JR (1972) Counterdiffusion of liquid hydrocarbons in type Y
- 646 zeolite: Effect of molecular size, molecular type, and direction of diffusion. *AIChE J*
- 647 18:816–824.
- 648
- 649
- 650
- 651
- 652
- 653
- 654
- 655
- 656
- 657
- 658
- 659
- 660
- 661
- 662
- 663
- 664
- 665
- 666
- 667
- 668
- 669
- 670
- 671
- 672
- 673
- 674
- 675
- 676
- 677
- 678
- 679
- 680
- 681
- 682

PNAS proof
Embargoed

683
684
685
686
687
688
689
690
691
692
693
694
695
696
697
698
699
700
701
702
703
704
705
706
707
708
709
710
711
712
713
714
715
716
717
718
719
720
721
722
723
724
725
726
727
728
729
730
731
732
733
734
735
736
737
738
739
740
741
742
743
744

AUTHOR QUERIES

AUTHOR PLEASE ANSWER ALL QUERIES

1

- Q: 1_Please contact PNAS_Specialist.djs@sheridan.com if you have questions about the editorial changes, this list of queries, or the figures in your article. Please include your manuscript number in the subject line of all email correspondence; your manuscript number is 201813849.
- Q: 2_Please (i) review the author affiliation and footnote symbols carefully, (ii) check the order of the author names, and (iii) check the spelling of all author names, initials, and affiliations. To confirm that the author and affiliation lines are correct, add the comment “OK” next to the author line. This is your final opportunity to correct any errors prior to publication. Misspelled names or missing initials will affect an author’s searchability. Once a manuscript publishes online, any corrections (if approved) will require publishing an erratum; there is a processing fee for approved erratum. Please check with your coauthors about how they want their names and affiliations to appear.
- Q: 3_Please review the information in the author contribution footnote carefully. Please make sure that the information is correct and that the correct author initials are listed. Note that the order of author initials matches the order of the author line per journal style. You may add contributions to the list in the footnote; however, funding should not be an author’s only contribution to the work.
- Q: 4_Please note that the spelling of the following author names in the manuscript differs from the spelling provided in the article metadata: Benjamin E. R. Snyder, Hannah M. Rhoda, Lars H. Böttger, and James J. Yan. The spelling provided in the manuscript has been retained; please confirm.
- Q: 5_You have chosen not to pay for the PNAS open access option. Please confirm that this is correct. If this is incorrect, and you would like to pay for the PNAS open access option, please note this in the margin, indicating whether you prefer CC BY or CC BY-NC-ND.
- Q: 6_Please note that all supporting information (SI) file(s), including the SI Appendix PDF and/or any other files (e.g., datasets, movies), have not been altered in any way and will be posted online as originally submitted. If you have any changes to your SI file(s), please provide new, ready-to-publish replacement files without annotations. If you are unable to view your SI files in the Author Center, or if you have any questions regarding your SI, please contact PNAS_Specialist.djs@sheridan.com.
- Q: 7_PNAS allows up to five keywords. You may add 2 keywords. Also, please check the order of your keywords and approve or reorder them as necessary.
- Q: 8_Per PNAS style, certain compound terms are hyphenated when used as adjectives and unhyphenated when used as nouns. This style has been applied consistently throughout where (and if) applicable.
- Q: 9_Please note the article title cannot begin with a general word such as “The” or “A.”
- Q: 10_PNAS does not allow claims of priority or primacy, hence the term “new” has been deleted

AUTHOR QUERIES

AUTHOR PLEASE ANSWER ALL QUERIES

2

- Q: 11_PNAS articles should be accessible to a broad scientific audience. As such, please spell out XANES.
- Q: 12_PNAS articles should be accessible to a broad scientific audience. As such, please spell out “rR.”
- Q: 13_PNAS articles should be accessible to a broad scientific audience. As such, please spell out ABS.
- Q: 14_Please rewrite sentence beginning “¹⁸O label incorporation” to avoid starting with a number.
- Q: 15_PNAS articles should be accessible to a broad scientific audience. As such, we have spelled out “RT” as room temperature. Please confirm.
- Q: 16_PNAS articles should be accessible to a broad scientific audience. As such, please spell out “DR” in “DR-UV-vis.”
- Q: 17_PNAS articles should be accessible to a broad scientific audience. As such, please spell out LUMO.
- Q: 18_PNAS articles should be accessible to a broad scientific audience. As such, please spell out FMO and delete the abbreviation, as it only appears once.
- Q: 19_Please spell out “H/D KIE.”
- Q: 20_PNAS articles should be accessible to a broad scientific audience. As such, please spell out
- Q: 21_PNAS articles should be accessible to a broad scientific audience. As such, please spell out BDE and delete the abbreviation, as it only appears once.
- Q: 22_Please confirm information added to ref. 1.
- Q: 23_Please verify that all et al. references contain 6 or more authors. If 5 authors or fewer, please supply complete author lists.
- Q: 24_Please confirm location for the publisher in ref. 5.
- Q: 25_Please provide volume number for ref. 6.
- Q: 26_Please provide location for the publisher in ref. 8.
- Q: 27_Please rewrite Fig. 1 legend beginning “⁵⁷Fe Mössbauer spectrum of α -O” to avoid starting with a number.
- Q: 28_Please rewrite Fig. 3C legend so it does not begin with a number.
- Q: 29_PNAS articles should be accessible to a broad scientific audience. As such, please spell out “LUMO.”
-
-